2D Node-Based Finite Element Method on Linear Accelerator Cavity for Radiation Therapy

Vinod Babu Pusuluri[1]*, A M Prasad[2], Naresh K Darimireddy[3]

[1]*Departmnt of ECE, JNTU Kakinada & RGUKT, Andhra Pradesh, India.* vinod@rguktn.ac.in

[2]*Department of ECE, JNTU Kakinad, Andhra Pradesh, India.* a_malli65@jntucek.ac.in

[3]*Department of ECE, Lendi IET(A), Jonnada, India.* yosuna@ieee.org

Abstract: This paper deals with the Electromagnetic (EM) field characterization of an S-band Linear Accelerator (LA) Cavity, which is extensively used in cancer treatment. The analysis of the proposed cavity is carried out using an Eigen-mode full-wave EM solver. Mathematical formulation of cavity parameters using the Finite Element Method up to the system of equations is presented. The EM formulization uses a simple 2D square box as segmentation element and also node-based basis functions are used inside the cavity than the edge-based functions. The proposed numerical analysis of a single cavity of LA system is also applicable for a system with multiple numbers of cavities. The cavity has a resonance of 3.0474 GHz and a Q-factor of 17181.6 with finite conducting boundaries at the ends of the drift tube. The nose cone structure in the cavity is essential to have a stronger E-field at the center where the beam passes. Further, the particle acceleration is not constant along the axis of the cavity, which may have severe consequences for beam dynamics. Proper beam dynamics in LA plays a key role in reducing the mortality rate in cancer therapy applications.

Keywords: Linear accelerators, mathematical modeling, Single Cavity, Numerical field calculations, High-frequency structure simulator, Finite Element Method.

1. INTRODUCTION

According to WHO (World Health Organization) reports, cancer is the second leading cause of death worldwide. The global cancer burden is estimated to rise by 18.1 million, with a death count of 10 million in 2020 and 9.6 million in 2021. One in five men and one in six women develop cancer during their lifetime, and one in 8 and one in 11 die for the same reason [1-2]. The common cancers are breast, lung, prostate, colon, and rectum. Tobacco use is the reason for 33% of cancer deaths, and high body mass index, consumption of alcohol, low fruit and vegetable intake, and lack of sufficient physical activity are other main reasons for this deadly disease. Cancer-causing infections such as human papillomavirus (HPV) and hepatitis are responsible for approximately 30% of cancer cases in low- and lower-middle-income countries. Though many cancers are curable and effective treatment is available if they are detected at early stages, it has become a longstanding life-threatening disease. As human life is of the utmost importance, it is a big challenge for the scientific community to find a possible global solution for this life-threatening disease.

Cancer is a general term for a large group of diseases that can affect any part of the human body. One defining feature of cancer is the creation of abnormal cells called malignant tumors or neoplasm that grow beyond the normal boundaries and can spread to other parts of the body within no time. The further stage in this process is called metastasis which is the prime cause of cancer death [3]-[4].

There are multiple ways to reduce the cancer risk factor. 30-50 % of present cancers can be prevented by avoiding cancer risk factors and implementing evidence-based prevention strategies in daily life. Cancer burden can also be reduced by early detection and proper treatment and care for the patient who develops cancer. A few preventable strategies for cancer are mentioned in literature [5].

The correct cancer diagnosis is essential for appropriate and effective treatment because every cancer type requires a specific treatment course of therapy. Treatment usually includes surgery, radiotherapy, and systemic therapy

(chemotherapy, hormonal treatments, and targeted biological therapies). Proper treatment regimen selection considers both the cancer and the individual being treated. Completing the treatment protocol in a defined period is important to achieve the predicted therapeutic result. The research groups and the medical world came up with a few possible treatments like Radiation therapy, Chemotherapy, Bone marrow transplantation, Immunotherapy, Hormone therapy, etc. One of the standard practices the current medical world using today to treat Cancer is Chemotherapy or Radiation Therapy, where high energy X-ray or electron beam are applied to the cancer cell [6].

In radiation therapy or radiotherapy, ionizing radiation is applied to kill or control the cancer cell/tumor. Radiation therapy is widely used if the malignant tumor is located in a fixed human body area. Here in radiation therapy the ionizing radiation is delivered to the cancer cell through a linear accelerator system. The ionizing radiation in radiation therapy kills the D.N.A. of malignant tumors, thereby; it reduces the growth of the tumors. Medical oncology explains chemotherapy as the application of multiple drugs on the malignant tissue of a cancer patient. Radiation therapy is the application of high-energy X-ray or particle beam to cancer cells. Once cancerous cell is identified based on its tissue characteristics, it will be divided into various small tissues. Once a group of small tissues is available, it would become easy for the medical experts to treat each small tissue by interacting with high energy X-ray or particle beam. The generation of the X-rays is done by using a particle accelerator[7]-[8].

Linear Accelerator (LINAC) is extensively used in cancer therapy, non-destructive testing, and rocket propellant applications. In LINAC, a charged particle acquires the energy while it moves in a linear patch through a series of cavities where the charged particle experiences velocity modulation. The e-beam, through velocity modulation, will collide with the target for the X-ray production or be used directly on the tumor. The collimators, positioned on the X-ray or extracted particle beam, are necessary to deliver radiation to cancer (conformal radiation therapy) precisely. A prototype view of 6MeV LINAC system for radiation therapy is shown in Figure.1.In many radiotherapy LINACs; magnetrons are used to feed the cavities for producing the Radiofrequency fields to accelerate the particles. The electron beam is sent in a series of cavities to experience velocity modulation in its journey toward the target. LINAC bunches the charged particle at a particular radio frequency; as they travel through a series of cavities for the final energy. Parameters like fields inside the cavity, quality factor, beam timing, energy spread, and shunt impedance, beam current and geometric characteristics of the LINAC system are essential for the analysis. Various LINAC devices and their parametric analysis are available in the literature [9]-[17].

The analysis of the linear accelerators which is used in cancer therapy is very much essential. The Electromagnetic study of any device is done by using complex Electromagnetic computations. Accelerating electric fields and cavity parameters like resonance frequency and Quality factor in standing wave Medical LINACs has been calculated using High-Frequency Structural Simulator (HFSS), a full wave electromagnetic simulator. The existing research has used Finite Difference time domain (FDTD), Finite Difference (FDM), Method of Moments (MoM), and Finite Elements Method (F.E.M.) so far to calculate the field parameters of the many computational problems [22-25]. Here in this article system of equations was obtained by many 2D square basis functions of electromagnetic solver F.E.M. The LINAC cavity and its field characteristics are also discussed. The introduction of more advanced Machine Learning algorithms adds additional scope for the analysis of the LINAC.

This article analyzes the single cavity parameters in S-band LINAC system for field distribution using a full-wave electromagnetic solver high-frequency structural simulator (HFSS). Benchmark analysis attempt is made for HFSS by using a two-dimensional square element as a meshing element and node-based basis functions than edge-based functions in FEM. The field distribution, resonance frequency, and quality factor of the LINAC cavity are obtained, and the benchmark analysis of HFSS is derived up to a system of equations by using 2 dimensional square mesh and node basis functions. The subsequent sections give a brief overview of the LINAC cavity.

2. CAVITY DESIGN

S-band microwave LINACs are extensively used in cancer therapy. These are standing wave types of structures where the adjacent accelerating cavities are excited in opposite phases. The cavities' dimensions are adjusted so that the electron simultaneously passes through the cavity and takes the electromagnetic field's reverse phase. Thus the synchronized electron will always find an accelerating field. A schematic cross-section view of the multiple cavity system and its side cavities is shown in Figure 2. The cavity dimensions were considered to have S-band LINAC, as shown in Figure 3, where L=50mm, Ø=30^0, rd=3mm, R=38.9mm, R_1=23.5mm, Lt=9.1mm [27]. The Side cavities and

coupling iris are necessary to distribute better R.F. power in the accelerating cavities providing the suitable coupling between them for optimum E-field and phase. The sweep around the simulator's axis helps to obtain three-dimensional views [28]-[29]. The cross-sectional view of the single cavity structure and three-dimensional views are shown in Figures 3 and 4. The following sections will discuss the boundary conditions and excitations of the cavity to obtain the cavity parameters.

Figure1. Schematic of LINAC System.[Ref-16]

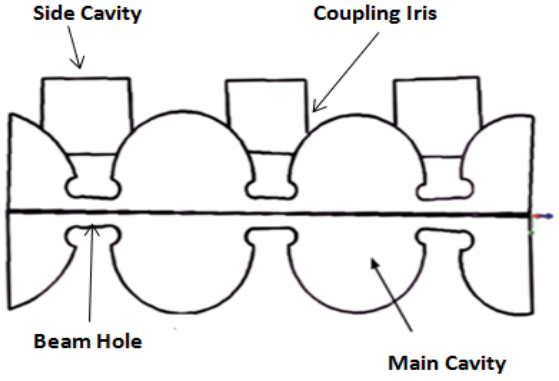

Figure 2. Schematic of Multiple cavity.

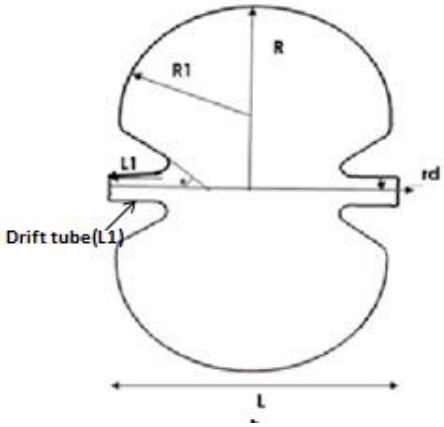

Figure 3. Cross sectional view of single cavity.

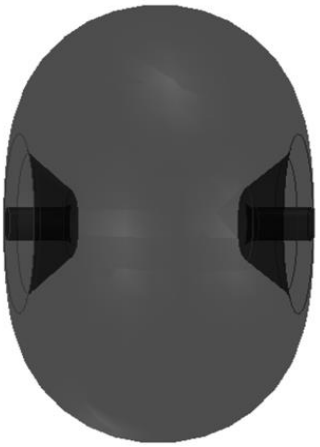

Figure 4. Simulated 3D design of single cavity

3. BOUNDARY CONDITIONS

The two-dimensional structure shown in Figure 3 is swept around the axis in HFSS to achieve three-dimensional one. This is a single cavity with perfect electric conductor boundaries on all sides except the axial hole through which the electron moves from one cavity to the next. Since the adjacent accelerating cavities are excited in opposite phases, the symmetry justifies the assumption of a perfect magnetic conductor along the hole. Application of the Eigen-mode solver of the simulator needs no input or excitation for the cavity. The subsequent chapters explain the computational electromagnetic approach through F.E.M. to achieve the fields inside the cavity [31]-[35].

A. System of Equations and F.E.M. approach

The implementation of numerical techniques generally leads to a system of equations, which in matrix notation is mentioned in Equation (1).

$$[A][X] = [b] \quad (1)$$

Where [A] is an augmented matrix which is a square matrix, and [b] is the right-hand side matrix, usually called the excitation and the solution is the unknown column vector, [X]. In the Eigen-mode solution [b] is λ[*X*].

Among all the solutions of Maxwell equation inside the cavity, we are interested in Transverse Magnetic modes because for accelerating beam a longitudinal E-field is required further, in TM mode all field quantities can be

expressed in terms of $H_{\emptyset}$. The cavities' cylindrical symmetry helps to achieve a prominent mode of interaction. Here in this analysis z-axis is the direction of the beam traveling. The expression for the field component is in Equation (2).

$$\nabla.(r\nabla H_{\emptyset}) + \left(rk^2 - \frac{1}{r}\right) H_{\emptyset} = 0 \quad (2)$$

Where 'k' is the wave number in free space at the resonant frequency, the above equation results from Maxwell's curl equation (source free case), and the "del" operator is given in the Equation (3), where subscripts 'u' represents the unit vectors

$$\nabla = \left(\frac{\partial}{\partial r}\right) u_r + \left(\frac{\partial}{\partial z}\right) u_z \quad (3)$$

The boundary conditions for the quarter wave cavity are $H_{\emptyset}$=0 on the axis due to singularity at r=0. $H_{\emptyset}$=0 at the end of the drift tube since the field points in opposite directions in neighboring linear axis cavities. Based on Image theory the normal derivative of the r*$H_{\emptyset}$ is zero on the metal boundaries and on vertical symmetric plane while considering the quarter part of the cavity since the modes in which field lines are perpendicular to the virtual edges are taken into consideration, which is given in Equation (4)

$$\frac{\partial(rH_{\emptyset})}{\partial n} = 0 \ (4)$$

Where 'n' is normal at the boundary.

B. Basic Steps of Proposed Single Cavity Design using F.E.M.

The F.E.M. analysis of any problem involves four significant steps.

a) Segmentation or meshing of the device geometry into a finite number of elements such that the dielectric is homogeneous in each element.

b) Deriving the governing equations for typical elements.

c) Assembly of all the elements of the device to generate the system of equations.

d) The solution of the system of equations is obtained to determine the unknowns.

The preference is given to the F.E.M. technique to analyze the LINAC system due to its optimized memory requirement and computational time. F.E.M. offers better computational efficiency with respect to FDM, M.O.M., and FDTD techniques [36-39].

The given device geometry in the present form is divided into several sub-problems that are easier to solve, i.e., the devices will be divided into a different number of finite elements. Here the finite elements are line segments or curved segments, two-dimensional (2D) triangles or squares, and three-dimensional (3D) tetrahedron bricks or hexagonal, as in Figure.5. The selection of the finite element shape depends on the effective area coverage of the device and mathematical simplicity. A simple rectangular shape or square is considered a finite element in the present cavity, as mentioned in Figure 5. The dimensions of the Finite elements will be in terms of the device wavelength in general, and it is on a tenth of the device wavelength (λ/10)[40]-[44]. The finite element segmented quarter-wave cavity is shown in Figures 6 and 7 respectively.

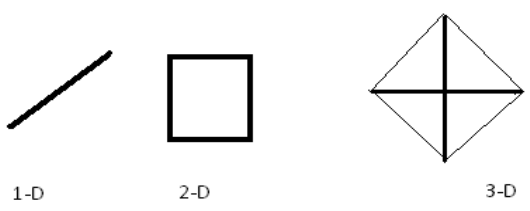

Figure 5. 1D, 2D, and 3D finite elements

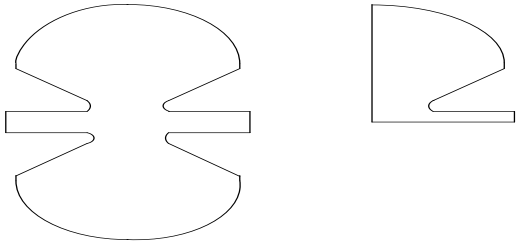

Figure 6. Single and Quarter Cavity

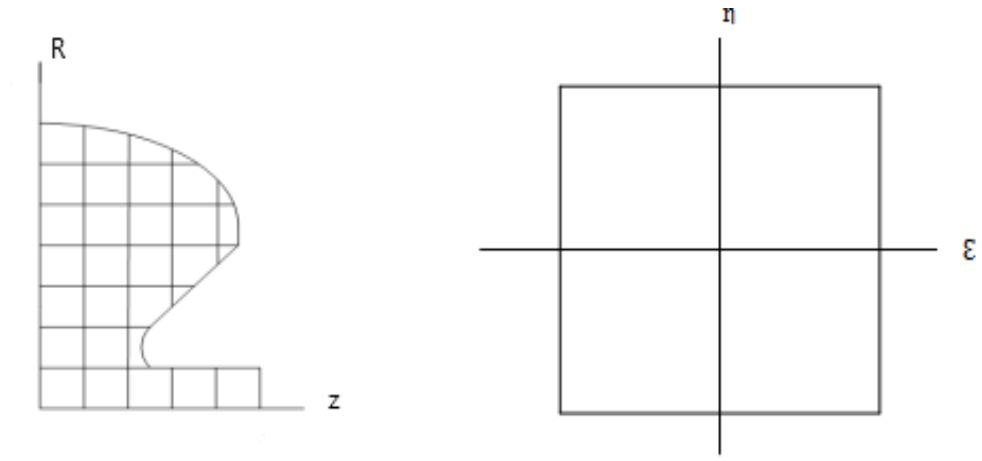

Figure.7 Segmented quarter cavity

The first box's horizontal and vertical length and basis function is mentioned using the following Equation (5) to (7).

$$r = \eta + \left(\frac{R}{2N}\right) + \left(\frac{R}{N}\right)(l-1) \quad (5)$$

$$z = \varepsilon + \left(\frac{Z}{2N}\right) + \left(\frac{Z}{N}\right)(k-1) \quad (6)$$

$$\alpha_{ii}(1) = \frac{1}{4}\left(1 + \frac{2N\varepsilon}{R}\right)\left(1 + \frac{2N\eta}{R}\right) \quad (7)$$

Where (l,k) is the number of squares in two different directions, R is the vertical length, and Z is the horizontal length. The center, the intersection point of ε and η, is considered a reference, N is the total number of nodes, and $i$indicates the node position. The basis functions at the remaining three corners are taken from the Equation (8) to (11).

$$\alpha_{(ii-\eta)} = \frac{1}{4}\left(1 + \frac{2N\varepsilon}{R}\right)\left(1 - \frac{2N\eta}{R}\right) \quad (8)$$

$$\alpha_{(ii-\varepsilon)} = \frac{1}{4}\left(1 - \frac{2N\varepsilon}{R}\right)\left(1 - \frac{2N\eta}{R}\right) \quad (9)$$

$$\alpha_{(ii-\varepsilon-\eta)} = \frac{1}{4}\left(1 - \frac{2N\varepsilon}{R}\right)\left(1 - \frac{2N\eta}{R}\right) \quad (10)$$

Now the basis function for the square box in the second quadrant is as follows.

$$\alpha_{ii}(2) = \frac{1}{4}\left(1 - \frac{2N\varepsilon}{R}\right)\left(1 + \frac{2N\eta}{R}\right) \quad (11)$$

The remaining three nodes for the second quadrant square are given in Equation (12) to (14).

$$\alpha_{(ii+\epsilon)} = \frac{1}{4}\left(1 + \frac{2N\varepsilon}{R}\right)\left(1 + \frac{2N\eta}{R}\right) \quad (12)$$

$$\alpha_{(ii-\eta)} = \frac{1}{4}\left(1 - \frac{2N\varepsilon}{R}\right)\left(1 - \frac{2N\eta}{R}\right) \quad (13)$$

$$\alpha_{(ii+\epsilon-\eta)} = \frac{1}{4}\left(1 - \frac{2N\varepsilon}{R}\right)\left(1 - \frac{2N\eta}{R}\right) \quad (14)$$

Similarly, the remaining two nodes' essential functions and the corner point are taken from the Equation (15) to (22).

$$\alpha_{ii}(3) = \frac{1}{4}\left(1 - \frac{2N\varepsilon}{R}\right)\left(1 - \frac{2N\eta}{R}\right) \quad (15)$$

$$\alpha_{(ii+\eta)} = \frac{1}{4}\left(1 - \frac{2N\varepsilon}{R}\right)\left(1 + \frac{2N\eta}{R}\right) \quad (16)$$

$$\alpha_{(ii+\epsilon)} = \frac{1}{4}\left(1 + \frac{2N\varepsilon}{R}\right)\left(1 - \frac{2N\eta}{R}\right) \quad (17)$$

$$\alpha_{(ii+\epsilon+\eta)} = \frac{1}{4}\left(1 + \frac{2N\varepsilon}{R}\right)\left(1 + \frac{2N\eta}{R}\right) \quad (18)$$

$$\alpha_{ii}(4) = \frac{1}{4}\left(1 + \frac{2N\varepsilon}{R}\right)\left(1 - \frac{2N\eta}{R}\right) \quad (19)$$

$\alpha_{(ii+\eta)} = \frac{1}{4}(1 + \frac{2N\varepsilon}{R})\ (1 + \frac{2N\eta}{R})$ (20)

$\alpha_{(ii+\epsilon)} = \frac{1}{4}(1 - \frac{2N\varepsilon}{R})(1 - \frac{2N\eta}{R})$ (21)

$\alpha_{(ii-\epsilon+\eta)} = \frac{1}{4}(1 - \frac{2N\varepsilon}{R})(1 + \frac{2N\eta}{R})$ (22)

$\varphi(x,y) = \sum_{e=1}^{N} \varphi^e(x,y)$ (23)

$\varphi^e(x,y) = \sum_{e=1}^{N} C_i^e \psi_i^e(x,y)$ (24)

Where, N is the number of node in the solution region, first equation representing the approximate field (potential) distribution,$\psi_i^e(x,y)$is the two-dimensional basic functions, and $C_i^e$is the unknown coefficient to be calculated? The expression for $C_i^e$is obtained by enforcing the differential equation for element as follows in Equation (25).

$\frac{\partial^2 \varphi^e}{\partial x^2} + \frac{\partial^2 \varphi^e}{\partial y^2} + k^2 \varphi^e = 0$ (25)

C. Formulation of F.E.M.:

Here a square element is considered the discrete element, and the original operator is projected into the linear space spanned by the basis functions. Here the projecting operator is L$H_{\emptyset}$=0, where in Equation (26)

$$\mathrm{L} = \nabla.(r\nabla) + (rk^2 - \frac{1}{r}) \qquad (26)$$

The basis function is $a_{j,m}$where (j, m) corresponds to the indices of the node along the Z-axis and along the r-axis, respectively. In F.E.M., there are two basis functions: edge-based and node-based basis functions here the proposed work is based on the node-based function. Now the function $H_{\emptyset}$ to be solved is expanded in terms of expansion co-efficient as given in Equation (27).

$$\boldsymbol{H_{\phi}} = \sum_{j,m} \boldsymbol{b_{jm} a_{jm}} \qquad (27)$$

The condition$\langle a_{jm}, LH_{\emptyset} \rangle = 0$ gives the expansion for the co-efficientb_{il}, where summation over$(i,l)$is over all values, giving non-zero contributions to the above integrals. Updating the Equation (1) with all the above coefficients will result in Equation (28).

$\sum_{i,l} b_{i,l} \int a_{i,l} a_{j,m} \left(rk^2 - \frac{1}{r}\right) ds = \sum_{i,l} b_{i,l} (\int r\, \nabla a_{i,l} \nabla a_{j,m}) ds + \sum_{i,l} b_{i,l} \int \sigma a_{i,l} a_{j,m} ds$ (28)

The values of E.M. parameters like resonance frequency and quality factor for various modes through the simulator are (3.0472 , 17181.6), (4.526, 18240) & (4.848,15.59) for Modes 1,2,3 respectively further; the Integral values required for the above expansion are tabulated in Tables 2, 3 and 4. To explain the field distribution inside the cavity, we need to have the Eigen-values of Equation (28) and σ helps us to achieve it.

4. DISCUSSION OF RESULTS

In this article, design of the single cavity is shown in Figure 4 in full-wave electromagnetic solver HFSS with proper boundary conditions is mentioned in the above sections. The field distribution inside the cavity is shown in Figure.8, where it is observed that the maximum field distribution is at the cavity nose cone. The cavity has a resonance frequency of 3.047GHz and 17181.6 quality factor. The field distribution is not uniform inside the cavity. Further, the resonance frequency and quality factor values vary for different modes, as reported in Table 1**.**The benchmark analysis is attempted for HFSS using 2D Square elements as mesh and node-based basis functions. The study of higher-order modes becomes simple using adaptive meshing at the nose cone structure rather than conventional. The system of equations through F.E.M. analysis is mentioned in Tables 2,3, and 4. The comparison of cavity parameters with the existing research is cited in Table .5.

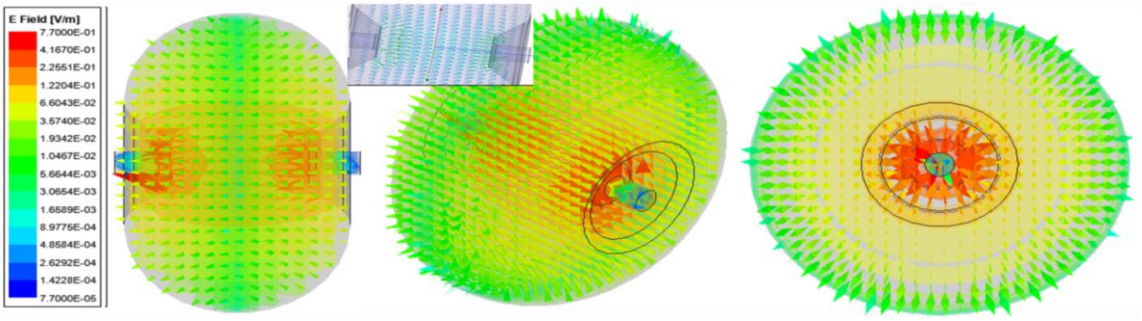

Figure 8. Field distribution inside the cavity of different orientations and with an inset view of end-to-end field distribution of cavity

Table 2. The values of $\int a_{jm} a_{il}$ r dA

I	*I*	$\int a_{jm} a_{il}$ r dA
j-1	m-1	$a^3(m-0.5)/36$
j-1	m	$a^3m/3$
j-1	m+1	$a^3(m+0.5)/36$
J	m-1	$a^3(m-0.5)/9$
J	m	$4a^3m/9$
J	m+1	$a^3(m+0.5)/9$
j+1	m-1	$a^3(m-0.5)/36$
j+1	m	$a^3m/9$
j+1	m+1	$a^3(m+0.5)/36$

Table 3. The values of $\int \nabla a_{jm} \nabla a_{il}$ r dA

I	*I*	$\int \nabla a_{jm} \nabla a_{il}$ r dA
j-1	m-1	-a(m-0.5)/3
j-1	m	-am/3
j-1	m+1	-a(m+0.5)/3
J	m-1	-a(m-0.5)/3
J	m	8am/3
J	m+1	-a(m+0.5)/3
j+1	m-1	-a(m-0.5)/3
j+1	m	-am/3
j+1	m+1	-a(m+0.5)/3

Table 4. Values of $\int a_{jm} a_{il}$ /r dA

I	*I*	$\int a_{jm} a_{il}$ /r dA
j-1	m-1	$a[\{1-4(m-0.5)^2\}\ln(m/(m-1))+4(m-0.5)]/24$
j-1	m	$a[\{1-4(m-0.5)+4(m-0.5)^2\}\ln(m/(m-1))+\{1+4(m+0.5)+4(m+0.5)^2\}\ln((m+1)/m)-8m]/24$
j-1	m+1	$a[\{1-4(m+0.5)^2\}\ln((m+1)/m)+4(m+0.5)]/24$
J	m-1	$a[\{1-4(m-0.5)^2\}\ln(m/(m-1))+4(m-0.5)]/6$
J	m	$a[\{1+4(m+0.5)-4(m-0.5)^2\}\ln(m/(m-1))+\{1+4(m+0.5)+4(m+0.5)^2\}\ln((m+1)/m)-8m]/6$

I	*I*	$\int a_{jm} a_{il} / r \, dA$
J	m+1	$a[\{1-4(m+0.5)^2\}\ln((m+1)/m)+4(m+0.5)]/6$
j+1	m-1	$a[\{1-4(m-0.5)^2\}\ln(m/(m-1))+4(m-0.5)]/24$
j+1	m	$a[\{1+4(m+0.5)-4(m-0.5)^2\}\ln(m/(m-1))+\{1+4(m+0.5)+4(m+0.5)^2\}\ln((m+1)/m)-8m]/24$
j+1	m+1	$a[\{1-4(m+0.5)^2\}\ln((m-1)/m)+4(m+0.5)]/24$

Table 5. The parametric and performance comparison

S.No	Ref.No	Energy	Cavity dimension (mm)	Quality factor	Resonance frequency(GHz)
1	16	6MeV	81	NA	2.98
2	18	4.5MeV	92	17379	2.87
3	20	27MeV	84	6180	3.0
4	Present work	6MeV	77.8	17182	3.047

5. CONCLUSIONS

The simulation result of the single cavity of LINAC using a high-frequency structural simulator indicates that the maximum field is observed at the nose cone structure of the cavity along the beam axis, as shown in Figure 8. The maximum electric field at the nose cone structure is due to increased capacitance at the cavity neck. Further, the field distribution is not uniform inside the cavity, and it has a resonance frequency of 3.0474 GHz, a quality factor of 17181.6. As the field is not constant and more capacitive at the cavity's entrance along the beam axis, it may have some consequences on beam dynamics. The cavity gap and the design of the nose cone structure must be carefully designed for the electric field, energy gradient-based, and other parameters based on the type of particle used. This creates a scope to change the cavity shape to achieve uniform field distribution. The exact values of the field, beam timing, energy spread, and shunt impedance, beam current and geometric characteristics of the LINAC system are essential to achieve a suitable beam for medical applications to reduce the mortality rate in cancer**.** These can be the subject of future study. The second part of this article gives the mathematical representation of the Finite Element Method solution up to a system of equations by taking a 2D square element as a meshing element and node basis function. Further, it is proposed to have adaptive meshing in case of higher order modes for better beam–field interaction.

6. REFERENCES

[1] Kimberly D. Miller et al.., Cancer treatment and survivorship statistics, 2022 A cancer Journal of Clinicians, vol 72, 409-436, Sep. 2022.

[2] Rebecca L. Siegel, Kimberly D. Miller, Hannah E. Fuchs, AhmedinJemal, "Cancer Statistics 2022",C.A. Cancer J Clin,2022;72:7-33.

[3] Alice Avancni et al.., "Exercise and Bone Health in Cancer: Enemy or ally," *MDPI Cancers,* 2022, 14(24),6078.

[4] Karol Bukowski, Mateusz Kciuk, and Renata Kontek, “Mechanisms of Multidrug Resistance in Cancer Chemotherapy”, *MDPI, Int.j.mol.sci.*2020. 21(9).

[5] WHO. Available online: https://www.who.int/news-room/fact-sheets/detail/cancer (accessed on 25 Jan. 2023).

[6] Nussbaumer, S.; Bonnabry, P.; Veuthey, J.L.; Fleury-Souverain, S. Analysis of anticancer drugs: A review. *Talanta* 2011, *85*, 2265–2289.

[7] Luqmani, Y.A. Mechanisms of drug resistance in cancer chemotherapy. *Med. Princ. Pract.* 2005, *14*, 35–48.

[8] Winnie M. C. van den Boogaardet al.., "Chemotherapy Side-Effects: Not All D.N.A. Damage Is Equal," MDPI Cancers, 2022, 14(3).

[9] A. Nassiri et al.., "History and Technology Developments of Radio Frequency (R.F.) Systems for Particle Accelerators" IEEE Transactions on Nuclear Science- 2015.

[10] Jorge Feuchtwangeret al.., "New Generation Compact Linear Accelerator for Low-Current, Low-Energy Multiple Applications," *MDPI, Appl.Sci.2022, 12(9).*
[11] Doyle, B.L.; McDaniel, F.D.; Hamm, R.W. The future of industrial accelerators and applications. *Rev. Accel. Sci. Technol.* 2019, *10*, 93–116.
[12] Indra J. Das,Poonam Yadav, andBharat B. Mittal, "Emergence of MR-Linac in Radiation Oncology: Successes and Challenges of Riding on the MRgRT Bandwagon" MDPI, *J. Clin. Med.* **2022**, *11*(17).
[13] Nikhil Rammohan, James W. Randall and Poonam Yadav, “History of Technological Advancements towards MR-Linac: The Future of Image-Guided Radiotherapy”MDPI,*J. Clin. Med.* **2022**, *11*(16), 4730.
[14] Linear Accelerators, CERN report CERN-2014-009 (CERN, Geneva, 2014).
[15] M. Hernandez et al.., "A 7MeV S-Band 2998MHz Variable Pulse Length Linear Accelerator System”, Proceedings of 2005 Particle Accelerator Conference, Knoxville, Tennessee.
[16] Andrey V. Mishin "Advances in X-Band and S-Band Linear Accelerator for Security, NDT, and other Applications," Proceedings of 2005 Particle Accelerator Conference, Knoxville, Tennessee.
[17] Byeong-No Lee et al.., "Beam Dynamics In 10 MeV S-band LINAC for Container Inspection System", Proceedings of IEEE conference 2013.
[18] N Nepal et al..," Design Study on Standing–Wave Linear Accelerator," Proceedings of the 2001 Particle Accelerator Conference, Chicago
[19] S. W. Jang et al.., “Development of a Low-*Q* Cavity-Type Beam Position Monitoring System," IEEETrans.Nucl. Sci, Vol. 64, No. 8, AUGUST 2017
[20] Dario Laneve et al.., "Electromagnetic Design of Microwave Cavities for Side-Coupled Linear Accelerators: a Hybrid Numerical/Analytical Approach," IEEE, Trans. 2018
[21] Y. S. Lee et al.., “X-band Linear Accelerator for Radiotherapy," KEIR report, 2008
[22] Marcel Ruf, Sven muller, Stefan Setzer, and Lorenz-Peter Schmidt,"Beam Position and Energy Monitoring in Compact Linear Accelerators for Radiotherapy," IEEE Trans on Biomedical Engg. VOL. 61, NO. 2, Feb. 2014.
[23] Wei Jiang, Na Liu, Tafi Tang, and Quin Huo Liu, "Mixed Finite Element Method for 2D vector Maxwell's Eigenvalue Problem in Anisotropic Medium" Progress in Electromagnetic Research, vol. 148, 159-170 2014.
[24] Qiang Ren, Luis E Tobon, and Quin Huo Liu,” A new 2D Non-Spurious Discontinuous Galerkin Finite Element Time Domain(DG-FETD)Method for Maxwell’s equations”, Progress in Electromagnetic Research, vol. 143, 385-404 2013.
[25] Quoc Khanh Nguyen, Stefano Serra-Capizzano, Cristina Tablino-Possio, and Eddie Wadbro, “Spectral Analysis of Finite Element Matrices Approximating 3D Linearly Elastic Structures and Multi Grid Proposals”, *MDPI Math. Comput. Appl. 2022, 27, 78.*
[26] Su Yan, Jian-mingJin, "Theoretical Formulation of a Time-Domain Finite Element Method for nonlinear magnetic problems in three dimensions," Progress in Electromagnetic Research, vol. 153, 33-55 2015.
[27] Rajat Roy and O Shanker, "Evaluation of Microwave LINAC cavity field parameters by the finite element method," Indian Journals of pure and applied Physics vol.30, pp. 207-210,1992.
[28] Rajat Roy and O. Shanker "Calculation of Inter cavity coupling coefficient for side coupled standing wave linear accelerator" IEEE Transactions on Microwave Theory and technologies vol. 41. No.6/7, June/July 1993.
[29] Subrata Das, et al..,“Linac for medical applications” 2009 IEEE Vacuum Electronics Conference-2009.
[30] Ramesh Garg "Analytical Computational methods in Electromagnetics," Artech House, 2008.
[31] R . Krishnan, A.P Deshpande, T.S Dixit, S.Chavan, C.S Nainwad. S-band 6MeV linac, Proceedings of PAC09, Vancouver B.C., Canada.
[32] Alzbeta E. Hartinger, Robert Guardo, Victor Kokta, Hervé Gagnon, "A 3-D Hybrid Finite Element Model to Characterize the Electrical Behavior of Cutaneous Tissues” *IEEE Transactions on Biomedical, Vol. 57 2010.*

DOI: https://doi.org/10.15379/ijmst.v10i1.2628